J. Fluid Mech. (2004), *vol.* 519, *pp.* 337–358. © 2004 Cambridge University Press
DOI: 10.1017/S0022112004001478 Printed in the United Kingdom

Slow spreading of fluid mud over a conical surface

By MASATOSHI YUHI[1] AND CHIANG C. MEI[2]

[1]Division of Environmental Science and Engineering, Graduate School of Natural Science and Technology, Kanazawa University, Kanazawa, Ishikawa, 920-8667, Japan

[2]Department of Civil and Environmental Engineering, Massachusetts Institute of Technology, Cambridge, MA 02139, USA

(Received 24 September 2003 and in revised form 26 July 2004)

We investigate the slow spreading of fluid mud over a gently sloped conical surface which may simulate a shallow basin or a hill. The mud is assumed to behave as a Bingham plastic possessing a finite yield stress and the lubrication approximation is used. Because of the finite yield stress, a variety of non-trivial equilibrium profiles can exist, corresponding to the state of deposit at the end of upward or downward motion. Analytical solutions are derived for axially symmetric deposits. It is shown that the front of the final profile in axisymmetric spreading is of a common form in dimensionless variables, independent of the total mud volume. Transient evolutions are then studied numerically by employing a finite-volume scheme for both axially symmetric and asymmetric spreading from a localized source. The characteristic features of the mud pile at different stages of spreading are examined. The final shape in asymmetric spreading is strongly affected by the total volume released and by the rate of discharge.

1. Introduction

Mud flows are frequent natural hazards in many regions of the world, and can be triggered by torrential rains, mountain slides or volcanic eruptions, sometimes leading to catastrophes (McDowell & Raymer 1986; Mileti *et al.* 1991; Takahashi 1991; Kang 1996). Fluid mud is typically a mixture of fine cohesive clay particles and water, and exhibits plastic-like behaviour in flows. Many past experiments have shown that the fluid mud behaves approximately as a Bingham-plastic when the clay concentration exceeds a few per cent by volume (e.g. Qian *et al.* 1985; Wang & Qian 1985). The spreading of a Bingham-like fluid with a free surface is also of interest to industrial processes of coating or pasting.

For three-dimensional flows, the constitutive relation of the Bingham fluid is well-known. Let τ_0 denote the yield stress, μ the Bingham viscosity, and τ_{ij} and ϵ_{ij} the stress tensor and the rate of strain tensor, respectively, the constitutive law reads:

$$\epsilon_{ij} = 0 \quad \text{if} \quad \tau \leqslant \tau_0 \tag{1.1}$$

and

$$\tau_{ij} = \left(\mu + \frac{\tau_0}{\epsilon}\right)\epsilon_{ij} \quad \text{if} \quad \tau \geqslant \tau_0, \tag{1.2}$$

where

$$\tau = \left(\tfrac{1}{2}\tau_{ij}\tau_{ij}\right)^{1/2}, \quad \epsilon = \left(\tfrac{1}{2}\epsilon_{ij}\epsilon_{ij}\right)^{1/2}, \tag{1.3}$$

https://doi.org/10.1017/S0022112004001478 Published online by Cambridge University Press

(see e.g. Prager 1961). In general, both the yield stress and the Bingham viscosity are empirical functions of the volume concentration of clay minerals and possibly the pH values and salinity (Krone 1963; Migniot 1968; Allersma 1980). The more refined Herschel–Bulkley model which combines the yield stress and power-law dependence has also been used by several authors in order to cover a broader range of shearing rates.

Because of the nonlinear rheological behaviour, early analytical or numerical studies of Bingham-like fluids are limited mainly to one- or two-dimensional spreading on an inclined plane. Liu & Mei (1989) have presented a two-dimensional theory for the unidirectional slow flow on a plane slope. Extension to a Herschel–Bulkley model has been made by Huang & Garcia (1998). For three-dimensional flows, the slow and steady spreading of mud released from a point source on a plane has been investigated by Hulme (1974) with a Bingham model, and by Coussot & Proust (1996) and Wilson & Burgess (1998) with a Herschel–Bulkley model. The static problem of the final deposit on an inclined plane has been studied experimentally by Coussot, Proust & Ancey (1996) and by Osmond & Griffiths (2001). For a horizontal plane bottom, Balmforth *et al.* (2000) have derived analytical and numerical solutions for the radially symmetric evolution of isothermal lava domes. Reviews of these topics can be found in Coussot (1997), Griffiths (2000) and Mei, Liu & Yuhi (2001). Balmforth *et al.* (2001, 2002) have developed an analytical theory for the equilibrium shape of lava domes on an inclined plane. For high-speed flows, Liu & Mei (1994) and Ng & Mei (1994) have examined the nonlinear formation of roll waves for a Bingham fluid and a power-law fluid, respectively. Similar problems on the avalanche of dry granules down an inclined plane have been reported by Wieland, Gray & Hutter (1999) and Pouliquen & Forterre (2002).

Studies of non-Newtonian fluid flows over complex terrains are relatively scarce. For steady uniform flows in open channels of width comparable to the depth, Johnson (1970) has given solutions for various cross-sections (see also Johnson & Rodine 1984). Using a Herschel–Bulkley model, Coussot (1997) has proposed an empirical formula for the discharge in an open channel of rectangular and trapezoidal cross-sections. Mei & Yuhi (2001) gave an approximate theory of three-dimensional transient spreading of a thin layer of Bingham fluid flowing down a wide and shallow open channel. Assuming slow flows, they used the lubrication approximation and examined several transient phenomena including stationary waves and the transient release and final deposition of mud piles, analytically and numerically.

In this paper, we shall extend our earlier work (Mei & Yuhi 2001) and investigate the effect of terrain on mudflow evolution. Specifically, we treat the slow spreading and stoppage of a Bingham-plastic fluid for two types of conical surface: a conical basin and a conical hill, both of small slope. For both geometries, the axially symmetric profile of threshold equilibrium will first be described analytically. The general cases of transient spreading are then studied numerically for both axially symmetric and asymmetric spreading from a localized source.

2. Governing equations

For a shallow layer of fluid spreading on a conical surface of finite inclination and vertical axis, we can, in principle, employ an orthogonal coordinate system so that distances and velocities are measured in either the tangential or the normal directions with respect to the conical surface. The approximate equations from a systematic but lengthy perturbation analysis are given in the Appendix. In nature, the slope of a

https://doi.org/10.1017/S0022112004001478 Published online by Cambridge University Press

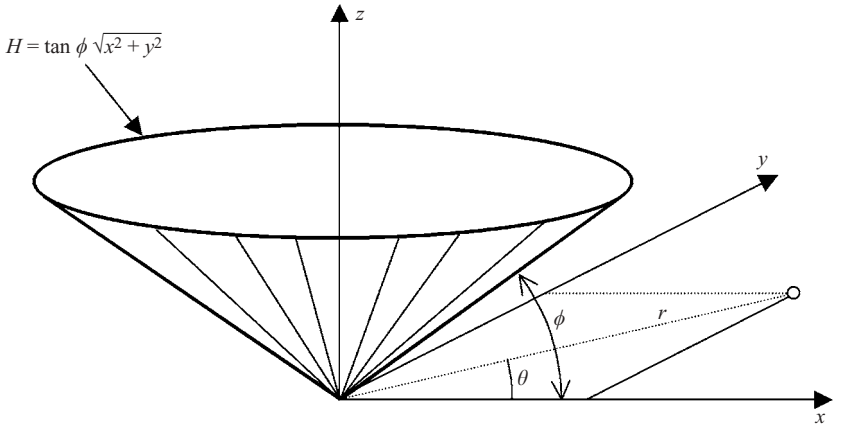


FIGURE 1. Definition sketch for the conical basin.

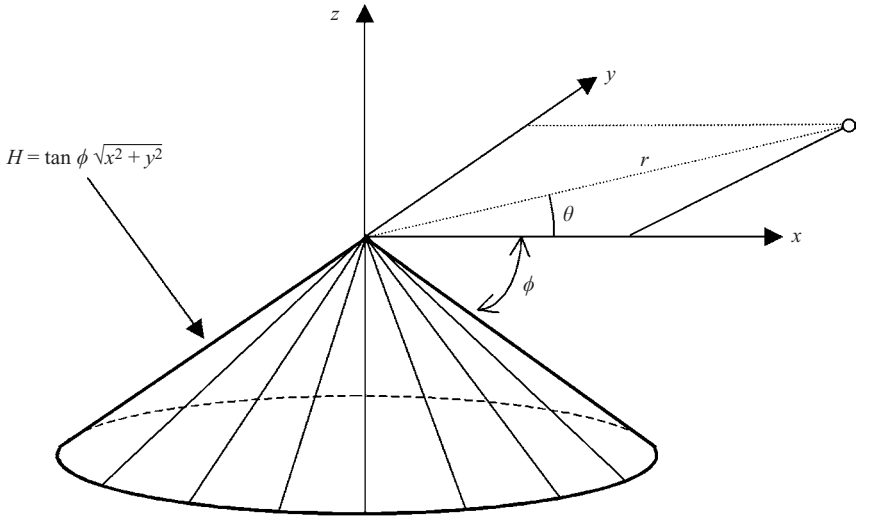


FIGURE 2. Definition sketch for the conical hill.

basin or a hill is often small; it is more convenient to use the cylindrical polar (r, θ, z) or the rectangular (x, y, z) coordinates with z pointing vertically upwards, as shown in figures 1 and 2. Let $z = H(r) = \pm r\tan\phi$ be the conical surface with $r = \sqrt{x^2+y^2}$, and $z = h(r, \theta, t)$ be the vertical coordinate of the free surface. The vertical mud depth is then $d = h - H$, which differs slightly from the thickness of the layer measured normally from the cone. Ignoring inertia and approximating the tangential stress components by the horizontal stresses, then

$$\tau_{xz} = -\rho g(h-z)\frac{\partial h}{\partial x}, \quad \tau_{yz} = -\rho g(h-z)\frac{\partial h}{\partial y}, \tag{2.1}$$

where ρ and g are the density of the fluid and the acceleration due to gravity, respectively. On the conical bed, the bed stress components are

$$\tau^b_{xz} = -\rho g(h-H)\frac{\partial h}{\partial x}, \quad \tau^b_{yz} = -\rho g(h-H)\frac{\partial h}{\partial y}. \tag{2.2}$$

https://doi.org/10.1017/S0022112004001478 Published online by Cambridge University Press

From the Bingham constitutive relation, the local bed shear stress must exceed the yield stress for flow to exist

$$\rho g(h-H)\left[\left(\frac{\partial h}{\partial x}\right)^2+\left(\frac{\partial h}{\partial y}\right)^2\right]^{1/2} > \tau_0. \tag{2.3}$$

Within the flowing mud there is a yield surface $z=h_0$ on which the shear stress equals the yield stress. Above the yield surface there is a region of plug flow†; below the yield surface the flow is sheared. The horizontal velocity components can be readily calculated, and used to find the depth-integrated law of mass conservation,

$$\frac{\partial h}{\partial t}+\frac{g}{\nu}\frac{\partial}{\partial x}\left[\left(-\frac{\partial h}{\partial x}\right)F\right]+\frac{g}{\nu}\frac{\partial}{\partial y}\left[\left(-\frac{\partial h}{\partial y}\right)F\right]=S(x,y,t), \tag{2.4}$$

where

$$F=\tfrac{1}{6}(3h-h_0-2H)(h_0-H)^2, \tag{2.5}$$

ν is the dynamic viscosity, and S is the source strength. The yield surface $z=h_0$ above which velocity shear is negligible, is given by

$$\rho g(h-h_0)\left[\left(\frac{\partial h}{\partial x}\right)^2+\left(\frac{\partial h}{\partial y}\right)^2\right]^{1/2}=\tau_0. \tag{2.6}$$

All motion stops when $h_0=H$. Formally, these equations have the same appearance as those for a horizontal bottom (see Mei & Yuhi 2001; Balmforth *et al.* 2002). These approximate equations are shown in the Appendix to be equivalent to the small-slope limit of the more general equations in conical coordinates. The above lubrication approximations for Bingham fluids have been justified in different ways by Liu & Mei (1990) and Balmforth & Craster (1999).

We adopt the critical depth $h_c=\tau_0/(\rho g\sin\phi)$ on an inclined plane as the characteristic depth, and choose $L=h_c\cot\phi$ to be the horizontal length scale with $\phi\ll 1$. Let us introduce the following normalized variables

$$\left.\begin{aligned}&(x,y)=h_c cot\phi(x',y'),\quad (z,h,h_0,H)=h_c(z',h',h_0',H'),\quad t=\frac{\mu\cot^2\phi}{\rho g h_c}t',\\&F=h_c^3F',\quad S=\frac{\rho g h_c^2}{\mu\cot^2\phi}S',\quad V=\left(h_c^3\cot^2\phi\right)V',\end{aligned}\right\} \tag{2.7}$$

where V denotes the total mud volume, to be prescribed for transient problems later. The dimensionless governing equations read, with primes omitted for brevity,

$$\frac{\partial h}{\partial t}+\frac{\partial}{\partial x}\left[\left(-\frac{\partial h}{\partial x}\right)F\right]+\frac{\partial}{\partial y}\left[\left(-\frac{\partial h}{\partial y}\right)F\right]=S, \tag{2.8}$$

where

$$F=\tfrac{1}{6}(3h-h_0-2H)(h_0-H)^2. \tag{2.9}$$

The yield surface height h_0 is given by

$$(h-h_0)\left[\left(\frac{\partial h}{\partial x}\right)^2+\left(\frac{\partial h}{\partial y}\right)^2\right]^{1/2}=1. \tag{2.10}$$

Motion stops when $h_0=H=\pm r$.

† This region is only approximately a plug flow at the leading order. At higher orders, the fluid is weakly sheared (Lipscomb & Denn 1984; Piau 1996; Balmforth & Craster 1999).

https://doi.org/10.1017/S0022112004001478 Published online by Cambridge University Press

3. Threshold equilibrium

As in plane flows (Liu & Mei 1989), the surface profile at the threshold of motion or stoppage can be found analytically for the case with radial symmetry. It is first necessary to distinguish the threshold of upward from downward motion. On the bed of a conical basin, $H = r$, mud on the verge of moving or stopping from moving up (down), experiences a positive (negative) shear stress. Thus, the threshold condition is

$$-(h-r)\frac{\partial h}{\partial r} = \pm 1 \quad \text{for} \begin{cases} \text{upward threshold,} \\ \text{downward threshold.} \end{cases} \tag{3.1}$$

On the surface of a conical hill, $H = -r$, mud about to move up (down) experiences a negative (positive) shear stress, hence the threshold condition is

$$(h+r)\frac{\partial h}{\partial r} = \pm 1 \quad \text{for} \begin{cases} \text{upward threshold,} \\ \text{downward threshold.} \end{cases} \tag{3.2}$$

Integration of these equations gives the following profiles:

$$h - h_* = \pm \ln\left(\frac{h - r \pm 1}{h_* - r_* \pm 1}\right) \quad \text{for} \begin{cases} \text{upward threshold,} \\ \text{downward threshold,} \end{cases} \tag{3.3}$$

on the bed of a conical basin, and

$$h - h_* = \pm \ln\left(\frac{h + r \pm 1}{h_* + r_* \pm 1}\right) \quad \text{for} \begin{cases} \text{upward threshold,} \\ \text{downward threshold,} \end{cases} \tag{3.4}$$

on the surface of a conical hill. In these formulae, h_* is the height of the free surface at the radius r_*. In cases where there is an edge at $r = R$ where the mud surface intersects the dry bed, it is convenient to choose r_* and h_* and define the mud depth d as follows,

$$\begin{aligned} &r_* = R,\ h_* = R,\ d = h - r \qquad \text{for a basin,} \\ &r_* = R,\ h_* = -R,\ d = h + r \qquad \text{for a hill.} \end{aligned} \tag{3.5}$$

We can rewrite (3.3) for a basin as

$$d + (r - R) = \pm \ln(1 \pm d), \quad r \lesseqgtr R; \quad d = 0, \quad R \gtreqless r; \tag{3.6}$$

and (3.4) for a hill as

$$d - (r - R) = \pm \ln(1 \pm d), \quad R \gtreqless r; \quad d = 0, \quad r \lesseqgtr R; \tag{3.7}$$

where the upper (lower) signs correspond to upward(downward) thresholds. In each case, the profile of the mud front is a simple function of the radial distance $r - R$ from the dry edge, wherever it is located.

We now examine the physical implications of these profiles.

(i) *Upward threshold in a basin*

Taking the upper signs, (3.6) describes the final deposit due to a finite mud influx from the bottom of a basin. The maximum height or depth $d_m = h_m$ occurs at the centre where $r = 0$, thus,

$$R = h_m - \ln(1 + h_m). \tag{3.8}$$

Typical free-surface profiles are shown in figure 3 for various values of h_m. The radius of the outer rim is, of course, greater if mud is deeper at the basin centre. Along the rim, the surface slope is large, signifying local breakdown of the long-wave

https://doi.org/10.1017/S0022112004001478 Published online by Cambridge University Press

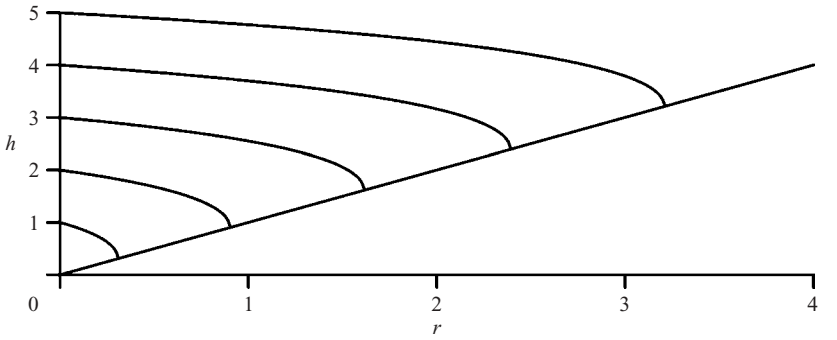


FIGURE 3. Upward thresholds in a conical basin for various maximum depths at the centre. In normalized form, all profiles near the edge are the same.

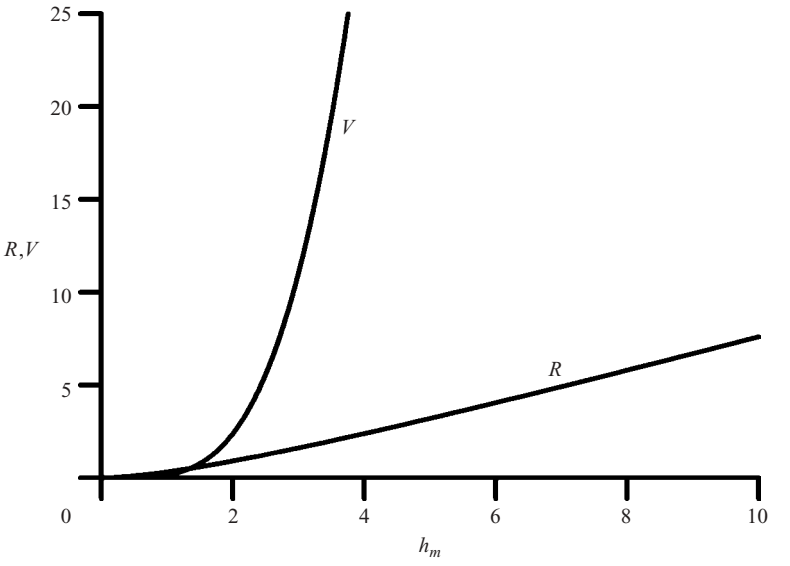


FIGURE 4. Dependence of R and V on h_m for the upward threshold in a conical basin.

approximation. As evidenced in experiments for similar examples in the plane case (Liu & Mei 1989), this local shortcoming has no significant global effects. The mud profile has a peak at the centre; the discontinuity of local slope is also a fault of the long-wave approximation. Similar peaks have been found before by Liu & Mei (1989) and Balmforth *et al.* (2000) in simpler situations and can, in principle, be made smoother by a higher-order analysis.

The relation between h_m and R (3.8) is plotted in figure 4. For large h_m, R increases almost linearly with h_m. Alternatively, we can relate h_m to the total mud volume V by

$$V = 2\pi \int_0^{R(h_m)} r(h - r)\,\mathrm{d}r. \tag{3.9}$$

This relation is also plotted in figure 4. The increase of V is very slow when h_m is less than unity, while for larger values of h_m the volume increases quite rapidly.

https://doi.org/10.1017/S0022112004001478 Published online by Cambridge University Press

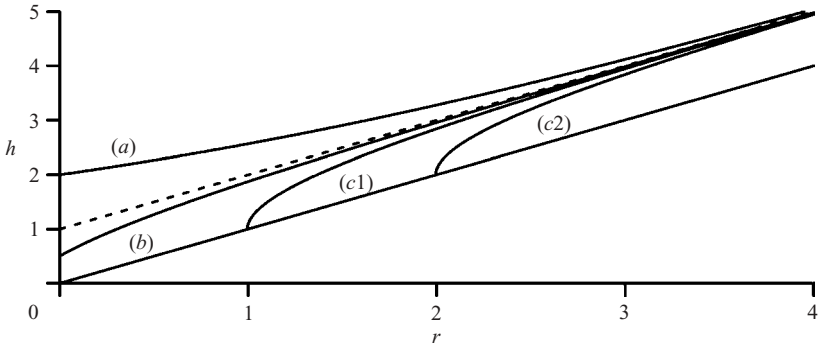


FIGURE 5. Downward threshold in conical basin. (*a*) sample case for $h_* > 1$ ($h_* = 2, r_* = 0$), (*b*) sample case for $h_* < 1$ and wet bottom ($h_* = 0.5, r_* = 0$). The broken line denotes the case of uniform thickness $h_* = 1, r_* = 0$, (*c*) sample cases for partially dry bottom, (*c*1): $R = 1$, (*c*2): $R = 2$.

(ii) *Downward threshold in a basin*

First, consider a basin completely covered by a thin layer of mud. At large r, the bottom approaches an inclined plane so that the normalized asymptotic depth must be equal to unity. (In dimensional form the asymptotic depth is equal to the critical depth h_c.) The mud profile is then given by (3.3) with the lower sign and h_* being the height (depth) at the centre $r = r_* = 0$. Two subcases can be distinguished. If the mud is thick at the centre: $h_* > 1$, the local mud depth decreases monotonically in r to the limiting value of unity at infinity. If the mud is thin at the centre: $h_* < 1$, the local depth increases instead. Sample results with $h_* = 2$ and 0.5 are shown by curves (*a*) and (*b*) in figure 5. If the centre thickness is unity, then it is uniform for all r, as shown by the broken line in figure 5.

Consider the next case where the basin centre within a circle $r < R$ is dry. The mud profile is given by (3.6) with the lower signs. It is easy to see that d approaches unity asymptotically as $r \to \infty$. Two sample profiles are shown in figure 5 for $R = 1$ and 2. For a large basin of finite radius, the value of R can be related to the total mud volume introduced from the rim. We stress again that the dimensionless profile of the mud front is always the same for all sizes of the dry circle at the basin centre.

(iii) *Upward threshold on a hill*

Let a rising sea of mud stop before covering the peak of a hill and the mud layer exists only outside the circle of radius $r = R$. Equation (3.7) with the upper signs applies and is shown in figure 6 for several values of $R > 0$. At large r, d becomes unbounded as r. If the mud sea stops rising after completely covering the hill, the final profile is obtained by setting $h = h_* > 0$ at $r = r_* = 0$ in (3.4) with the upper signs. Typical surface profiles are shown in figure 6, in which a pointed depression is present at the centre, a sign of Bingham-like fluids.

(iv) *Downward threshold on a hill*

Let the draining sea of mud stop before exposing the peak of a hill. If mud height at the hill peak is still finite, i.e. complete submergence, $h_* = h_m > 0$ at $r = r_* = 0$, the profile is given by (3.4) with the lower signs and $r_* = 0$. This profile is depicted for $h_m = 1.5$ in figure 7.

https://doi.org/10.1017/S0022112004001478 Published online by Cambridge University Press

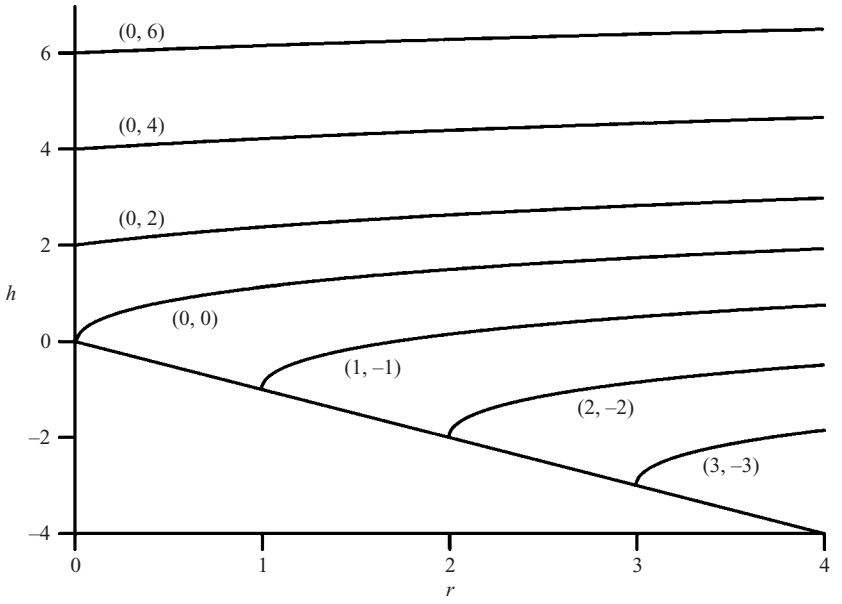


FIGURE 6. Upward threshold on conical hill. The first and second values in the parentheses denote r_* and h_*, respectively.

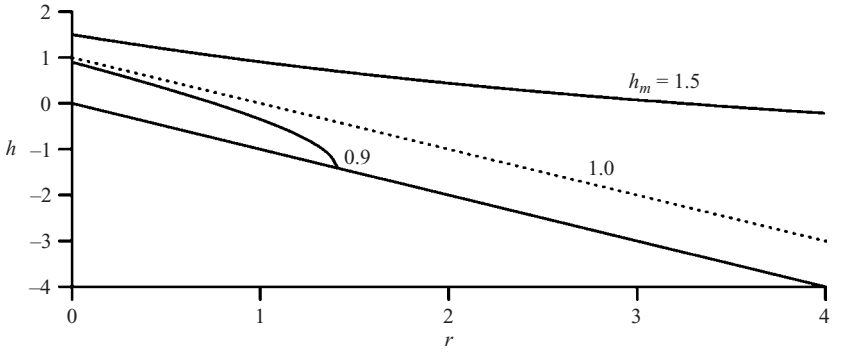


FIGURE 7. Downward threshold on conical hill.

For $h_m < 1$, the hill is dry outside the radius R. The maximum depth h_m at the peak $r = 0$ is found from (3.7) with lower signs,

$$R = -h_m - \ln(1 - h_m). \tag{3.10}$$

This can be the final deposit due to a finite mud influx from the apex of a hill. The relation between the maximum radius R and h_m is shown in figure 8. R increases rapidly to infinity when h_m approaches unity. The corresponding mud volume V is plotted in figure 8. Of course, an infinite volume of mud is required to cover the entire hill slope to the uniform depth $d = 1$.

4. Numerical scheme for calculating transients

For the transient spreading of mud, we employ the numerical method of finite volume described by Mei & Yuhi (2001). Briefly, a staggered mesh system is introduced

https://doi.org/10.1017/S0022112004001478 Published online by Cambridge University Press

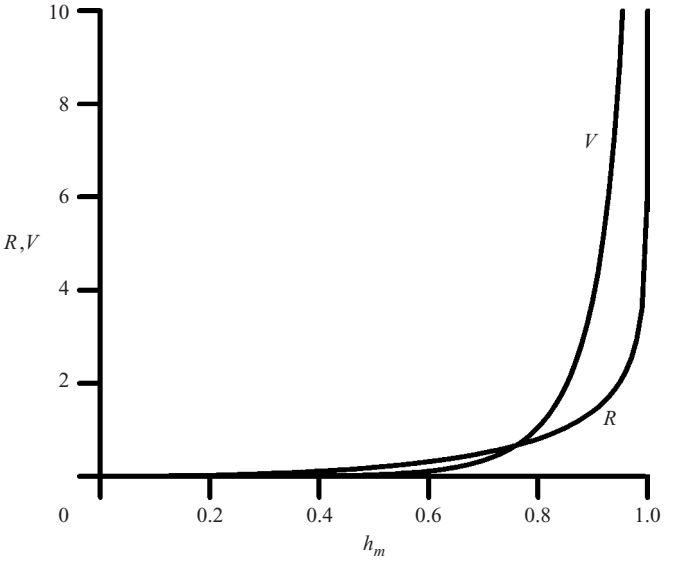


FIGURE 8. Dependence of R and V on h_m for the downward threshold on a conical hill.

for spatial discretization, and all spatial derivatives are approximated by second-order central differences. For time stepping, we employ the ADI (alternating direction implicit) scheme of second-order accuracy (Douglas 1955; Peaceman & Rachford 1955). Computations are carried out on a fixed grid, while the free boundary of the flow region is tracked in the course of computations. The numerical domain is taken to be sufficiently large so that the rim of deposit is always within the numerical boundaries. After testing for convergence by reducing the grid size, the typical grid size used in the calculations is $\Delta x = \Delta y = 0.01 \sim 0.025$ and $\Delta t = 10^{-4} \sim 10^{-2}$. The fluid is slowly discharged from a point source over a finite duration from $t = 0$ to $t = T_0$ so that

$$S = \begin{cases} Q_0 \delta(x - x_s)\delta(y - y_s), & 0 < t < T_0, \\ 0, & t > T_0, \end{cases} \tag{4.1}$$

where $(x, y) = (x_s, y_s)$ denotes the centre of the source, $Q_0 = V_0/T_0$ the discharge rate and V_0 is the total volume released. Computation is continued until the final state of rest (usually after $10T_0$ or $20T_0$). In computations, the source area is a small rectangle of sides equal to 3 numerical grids (i.e. $3\Delta x \times 3\Delta y$). It has been confirmed that the size of the source area has little influence on the final results. The validity of the numerical scheme has been confirmed through comparison with experiments and analytical solutions for the stationary waves down a inclined plane and an inclined channel (Mei & Yuhi 2001). To further confirm the numerical scheme for flows from a point source, we compare the computed large-time limit with the final static profile obtained analytically by Balmforth *et al.* (2001, 2002) for mud spreading on an inclined plane. Excellent agreement is found.

The three non-dimensional parameters governing the flow are: source location (x_s, y_s), discharge rate $(Q_0 = V_0/T_0)$, and the total volume (V_0). Computations have been performed for a range of all three parameters for both the axisymmetric and asymmetric spreading, but only a part of the results will be presented here.

https://doi.org/10.1017/S0022112004001478 Published online by Cambridge University Press

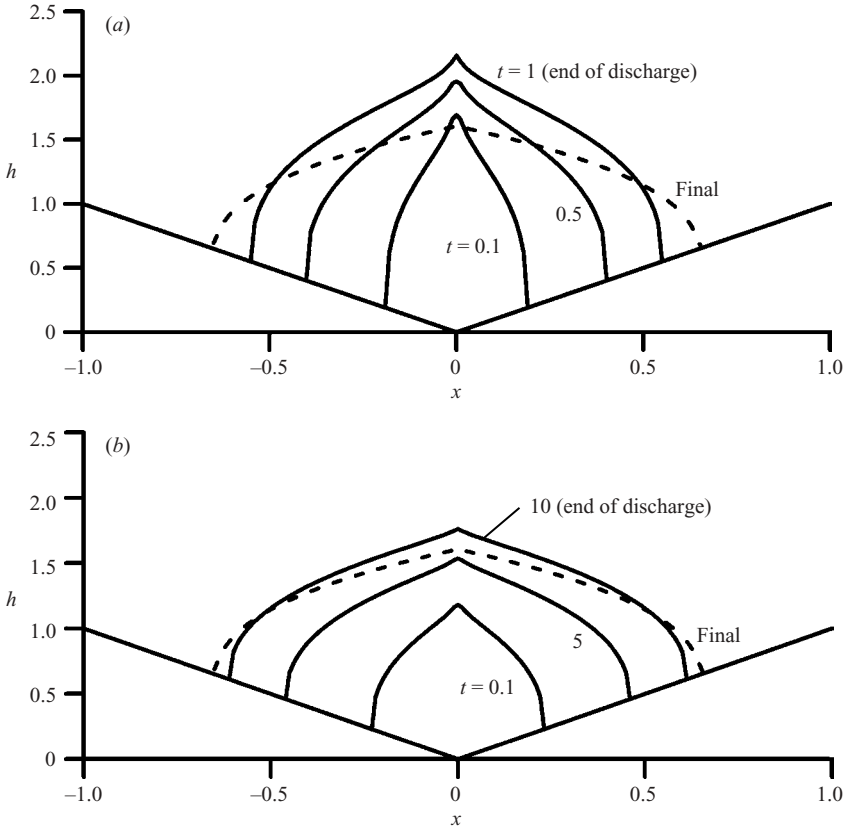


FIGURE 9. Time evolution of the free surface for $V_0 = 1$. The source is at $x_s = 0$, $y_s = 0$ (axisymmetric spreading). Discharge is terminated at $t = T_0 = 1$ and 10, respectively. (*a*) $Q_0 = V_0/T_0 = 1$. (*b*) $Q_0 = V_0/T_0 = 0.1$.

5. Transient spreading and deposition in a basin

For the simplest case of axial symmetry, $x_s = y_s = 0$, we display the evolution of mud in figure 9, for two different discharge rates, $Q_0 = 1$ and 0.1, while the total volume is the same ($V_0 = 1$). The corresponding time variation of the maximum height (h_m) and the front location (x_f) are shown in figure 10. From the beginning to the final stoppage, mud spreads outward with a pinnacle above the source. The transient mud profile is flatter for the slower discharge rate. After the discharge is long over, however, the final profiles in both cases are the same axisymmetric profile predicted by (3.3) with the upper sign, as described in figure 9. Clearly, the final profile of axisymmetric spreading is determined by the total volume only, and is independent of the discharge rate.

If the source is away from the centre, the spreading is asymmetric. Sample free surface evolution for asymmetric spreading is first shown in the left-hand column of figure 11 for a relatively small volume $V_0 = 1$ released from $(x_s, y_s) = (-1, 0)$. The discharge rate is set as $Q_0 = V_0/T_0 = 1$. Note that since the surface velocity (plug velocity) is described as

$$u_p(x, y, t) = -\frac{1}{2}\frac{\partial h}{\partial x}(h_0 - H)^2, \quad v_p(y, t) = -\frac{1}{2}\frac{\partial h}{\partial y}(h_0 - H)^2, \tag{5.1}$$

https://doi.org/10.1017/S0022112004001478 Published online by Cambridge University Press

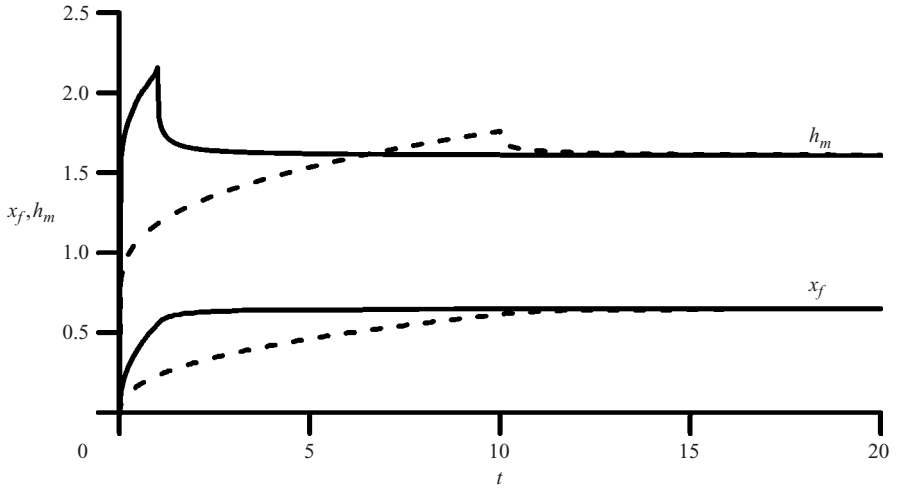


FIGURE 10. Time variation of the maximum height (h_m) and the front location (x_f). Solid lines : $Q_0 = 1$; broken lines : Q_0=0.1. The total volume is $V_0 = 1$. Discharge is terminated at $t = T_0 = 1$ and 10, respectively. Note the rapid decrease of h_m when discharge ends.

the direction of flow is normal to the height contours in the right-hand column of the figure. In the initial stage, the mud spreads out nearly uniformly in all directions, but soon after, the down-slope advance becomes faster than the lateral spreading. The pile becomes more elongated as time goes on. During the discharge, the pile has a peak above the source. After the discharge is over, the peak height decreases rapidly. On the rear side, the threshold equilibrium is approached. The front continues to move downward, resulting in the final shape of a tear drop. Being affected by the concave bottom topography, a shallow bowl is formed at the centre, bounded at the rear by a short ridge. A similar ridge can be seen in the experiments by Balmforth *et al.* (2002) for a pile released on an inclined plane.

We then show in figure 12 the evolution of a pile with a larger volume $V_0 = 27$ released from $(x_s, y_s) = (-3, 0)$. The rate of discharge is the same as before, $Q_0 = V_0/T_0 = 1$, so that discharge ends at $T_0 = 27$. The history of the front $(x_f - x_s)$, the rear $(x_r - x_s)$, and the maximum half-width (y_m) is shown from $t = 0$ to 50 in figure 13. Also included is the variation of the maximum depth, d_m. While both the downward advance and the lateral expansion are fastest at the very beginning, the downward motion is more prominent throughout most of the spreading process, resulting in a pointed front. When the front reaches the basin centre near $t = 10$, its advance is slowed down owing to the sudden variation of the slope. Mud then starts to rise over the bottom and the front is now more rounded. The maximum depth around (0, 0) also begins to increase again; mud is accumulated around the centre. The final equilibrium is approached shortly after the discharge is stopped.

The mud evolution can be seen through the profiles of the centreline ($y = 0$) in figure 14. As the total mud volume increases owing to the influx, the peak near the source rises, but soon falls after the discharge is ended. After mud covers the basin centre, a short ridge is formed near the source, but moves upward in time. Being in the plane of symmetry $y = 0$, the final equilibrium profile of the centreline is one-dimensional, hence is the same as for a mud layer on an inclined plane (Liu & Mei 1989). Referring to figure 15, we treat the two sides $x > 0$ and $x < 0$ separately. The final centreline profile is composed of three segments. The segment in the range of

https://doi.org/10.1017/S0022112004001478 Published online by Cambridge University Press

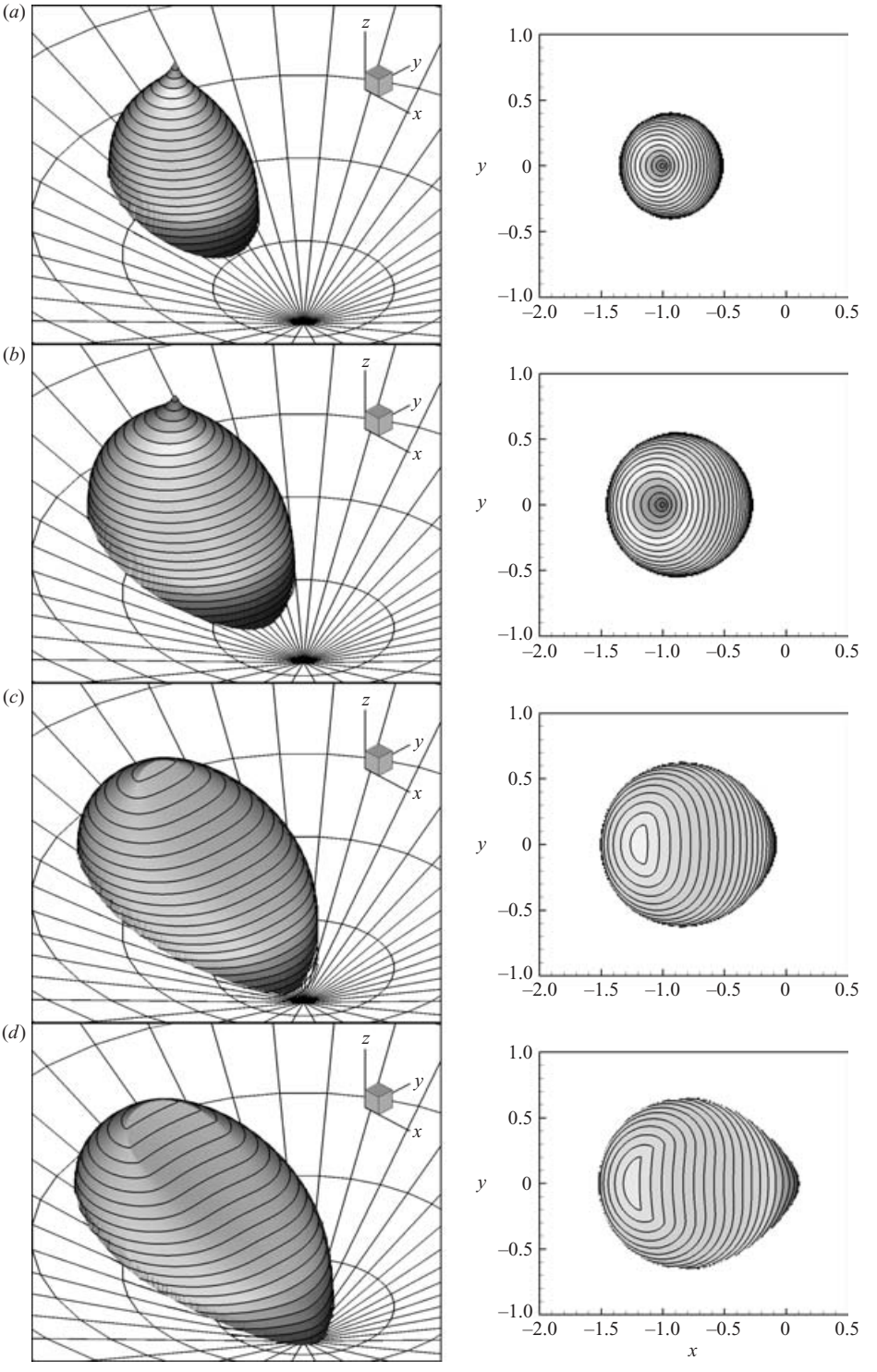


FIGURE 11. Time evolution of mudflow for $V_0 = 1$ and $Q_0 = 1$. (*a*) $t = 0.5$, (*b*) 1, (*c*) 2, (*d*) 20. The source is at $x_s = -1$, $y_s = 0$. Discharge is terminated at $t = 1$. In the right-hand column the contour lines of the free-surface height are plotted with the interval $\Delta h = 0.1$. The highest contour is (*a*) $h = 2.7$, (*b*) $h = 2.8$, (*c*) $h = 2.2$, (*d*) $h = 2.1$, respectively.

https://doi.org/10.1017/S0022112004001478 Published online by Cambridge University Press

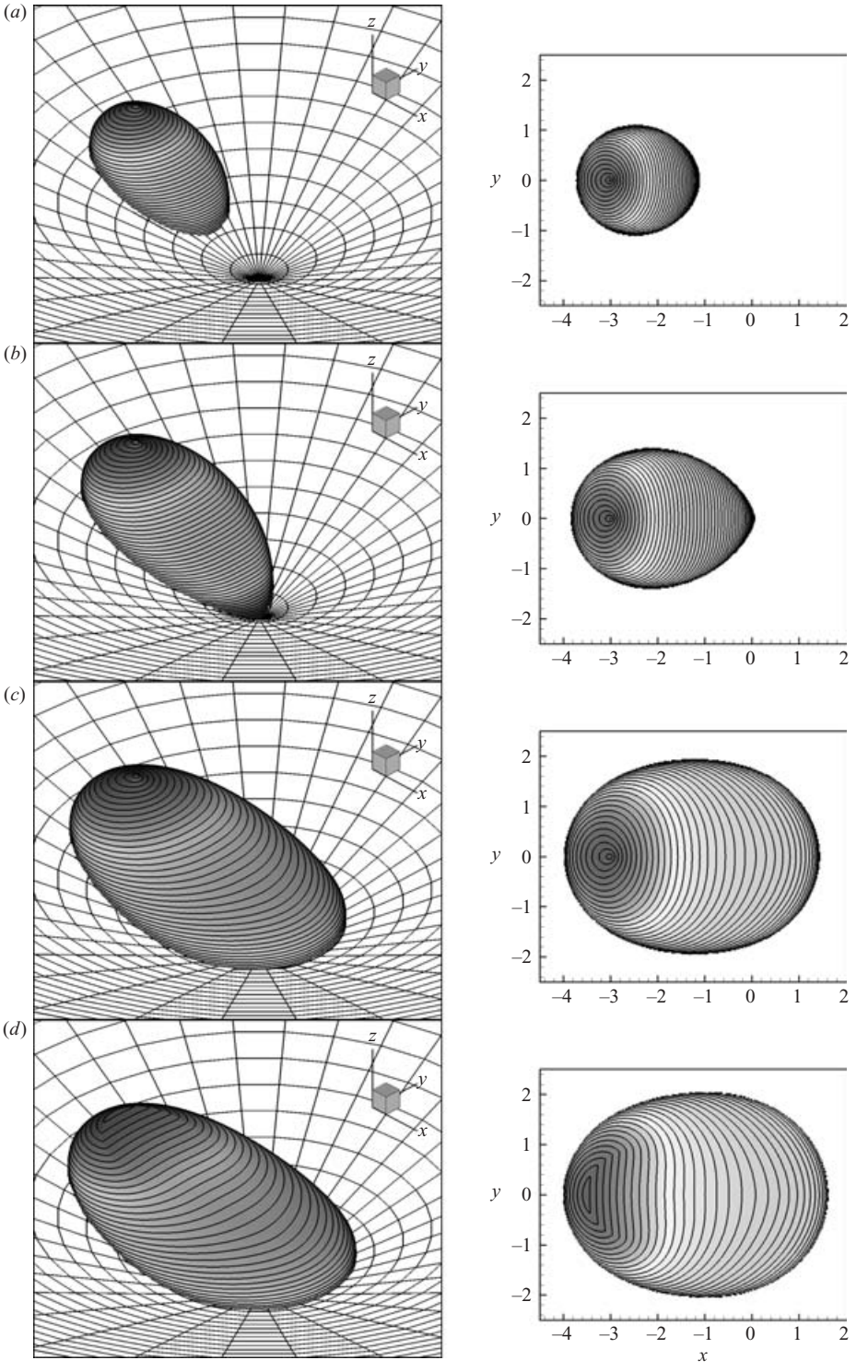


FIGURE 12. Time evolution of mudflow for $V_0 = 27$ and $Q_0 = 1$. (*a*) $t = 5$, (*b*) 10, (*c*) 27, (*d*) 100. The source is at $x_s = -3$, $y_s = 0$. Discharge is terminated at $t = 27$. In the right-hand column the contour lines of the free surface height are plotted with the interval $\Delta h = 0.1$. The highest contour is (*a*) $h = 5.0$, (*b*) $h = 5.1$, (*c*) $h = 5.2$, (*d*) $h = 4.8$, respectively.

https://doi.org/10.1017/S0022112004001478 Published online by Cambridge University Press

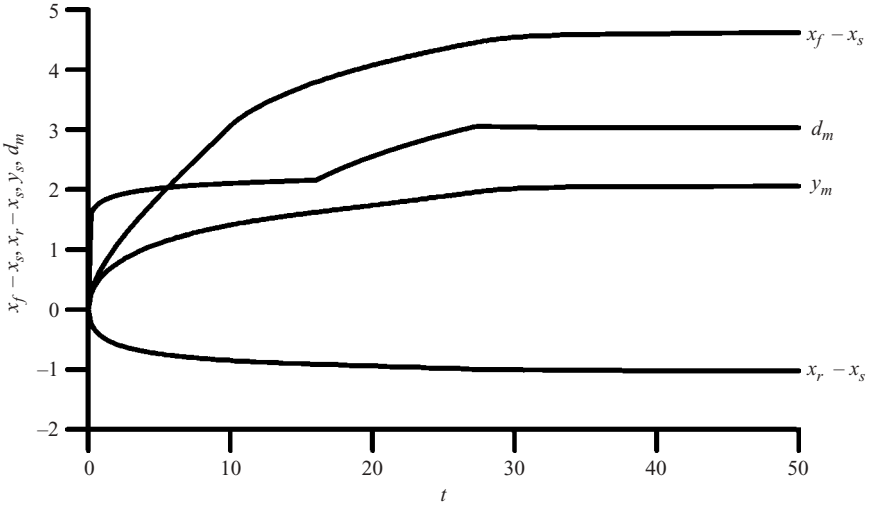


FIGURE 13. Time variation of front, back, side edge location, and maximum depth for $V_0 = 27$ and $Q_0 = 1$. The source is at $x_s = -3$, $y_s = 0$. The discharge is terminated at $t = 27$.

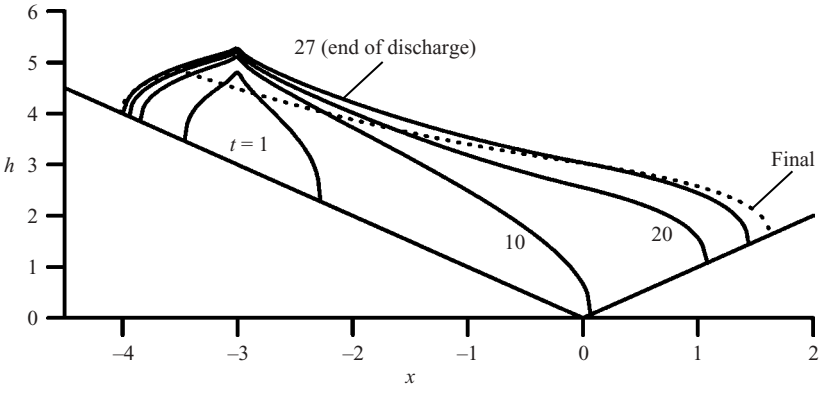


FIGURE 14. Time evolution of the centreline profile for $V_0 = 27$ and $Q_0 = 1$. The mud is discharged from $t = 0$ to $t = 27$. The source is at $x_s = -3$, $y_s = 0$. The final profile is obtained at $t = 500$.

$0 < x < x_f$ is convex upward. Since mud is at the end of climbing uphill with $\partial h/\partial x < 0$, we use the upper sign in (3.3) and take $x_* = h_* = x_f$ to obtain the mud profile

$$h - x_f = \ln(h - x + 1) \quad \text{for} \quad 0 < x < x_f. \tag{5.2}$$

The segment in the centre region $x_m < x < 0$ is concave upward. Here, mud is at the end of sinking along a plane slope. By taking the lower sign of (3.3) with $h_* = h_m$ and $x_* = x_m$, the profile is given by

$$h - h_m = -\ln\left(\frac{h + x - 1}{h_m + x_m - 1}\right) \quad \text{for} \quad x_m < x < 0. \tag{5.3}$$

Finally, the segment in $x_r < x < x_m$ is convex upward, and corresponds to the end of climbing a plane slope. The profile is

$$h - h_m = \ln\left(\frac{h + x + 1}{h_m + x_m + 1}\right) \quad \text{for} \quad x_r < x < x_m, \tag{5.4}$$

https://doi.org/10.1017/S0022112004001478 Published online by Cambridge University Press

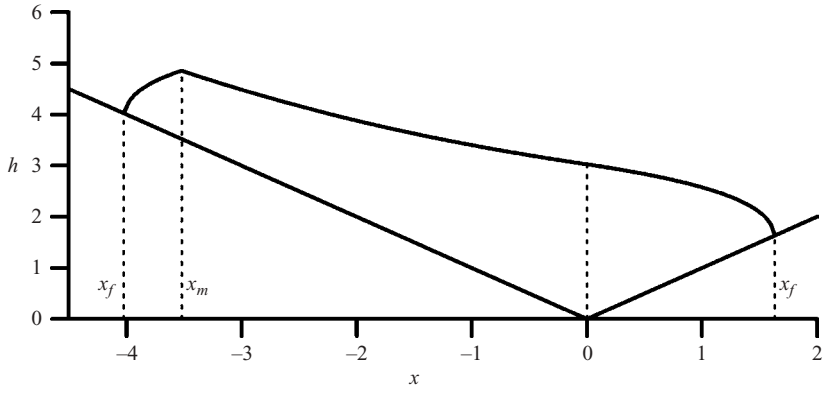


FIGURE 15. The final centreline profile for $V_0 = 27$ and $Q_0 = 1$. The source is at $x_s = -3$, $y_s = 0$. Numerical and analytical results are indistinguishable.

(cf. (3.4) with upper signs). By using the numerical values $x_f(=1.63)$, $x_m(=-3.52)$, and $h_m(=4.86)$ computed from the initial-value problem, analytical profiles in the three segment can be collected to yield the composite profile as shown in figure 15. This composite profile agrees with the computed final centreline profile at all points.

Finally, the effect of discharge rate in asymmetric spreading is investigated. In figure 16, we display the final free-surface profiles for two discharge rates, $Q_0 = 0.1$ and 10.0. In both cases, the total volume is $V_0 = 27$ and the source location is $(x_s, y_s) = (-3, 0)$, i.e. the same as in figure 12. When the discharge rate is high, spreading to the rear is significant; downward advance is small, resulting in a narrow front. On the other hand, when the discharge rate is small, the mud goes further downward, and has a wide front and narrow rear. Thus, the discharge rate affects the final shape, in contrast to the axisymmetric case.

6. Transient spreading and deposition on a hill

When the source is located at the peak, spreading is axisymmetric. Typical evolutions of the free surface and the yield surface are shown in figure 17, for $V_0 = 1$, $Q_0 = V_0/T_0 = 1$. The profiles are plotted for $t = 0.1$, 0.5, 1.0 (end of discharge) and 20 (final profile). Since the yield surface is related to the free surface according to (2.10) by

$$h_0 = h - \frac{1}{|\partial h/\partial r|}, \tag{6.1}$$

the free surface and the yield surface nearly coincide close to the front where the surface slope is very large (a local shortcoming of the approximation). For large t, the profile approaches that predicted by (3.7) with lower signs. After the discharge is over, the peak drops rapidly so that mud from the hilltop is drained to supply the downhill flow. Then the flow becomes extremely slow until the final equilibrium. Because of the radial spreading, the large decrease in mud depth near the source yields only a relatively small advance at the front. The final threshold profiles agree very well with the analytical prediction. It is also confirmed that the final profile of axisymmetric spreading on the hill is determined solely by the total volume, and is independent of the discharge rate, as in the case of a basin.

When the discharge is originated from the hillside, axisymmetry is lost. A typical example is shown in figure 18 for $V_0 = 1$, $Q_0 = 1$ released at $(x_s, y_s) = (1, 0)$. In the

https://doi.org/10.1017/S0022112004001478 Published online by Cambridge University Press

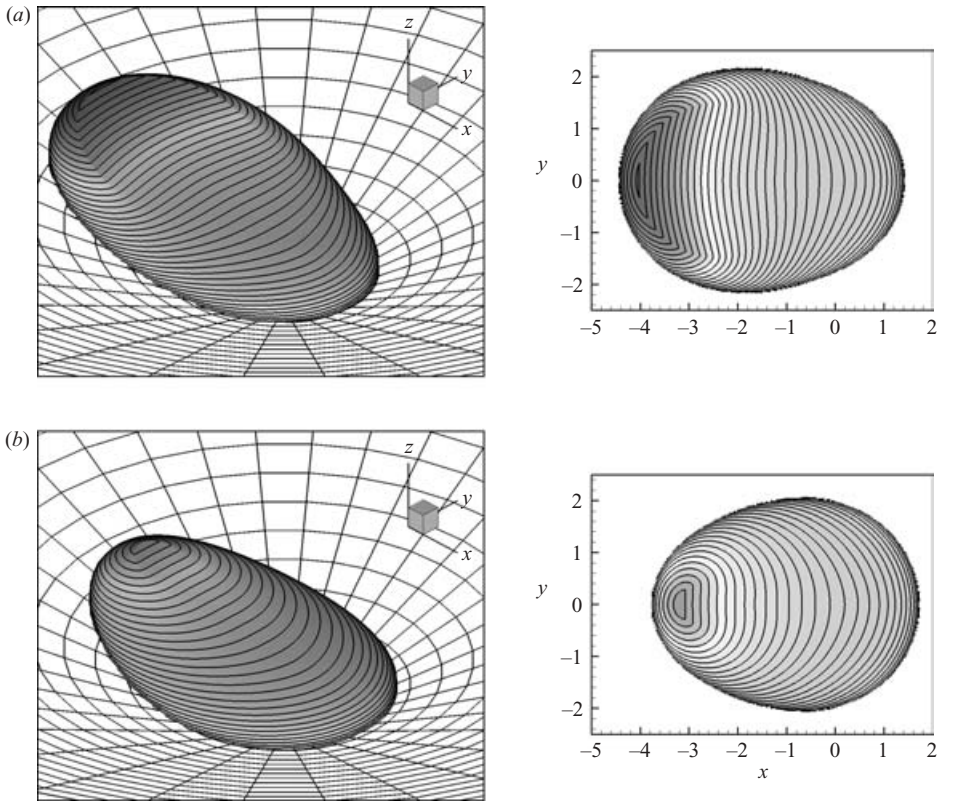


FIGURE 16. The final free-surface profile for $V_0 = 27$ and $(x_s, y_s) = (-3, 0)$. (*a*) High discharge rate, $Q_0 = 10$; (*b*) low discharge rate, $Q_0 = 0.1$. Discharge is terminated at $t = T_0 = 2.7$ and 270, respectively. The final shape is taken at $t = 50$ and 500, respectively. In the right-hand column the contour lines of the free surface height are plotted with the interval $\Delta h = 0.1$. The highest contour is $h = 5.2$ and $h = 4.6$ in the upper and lower figure, respectively.

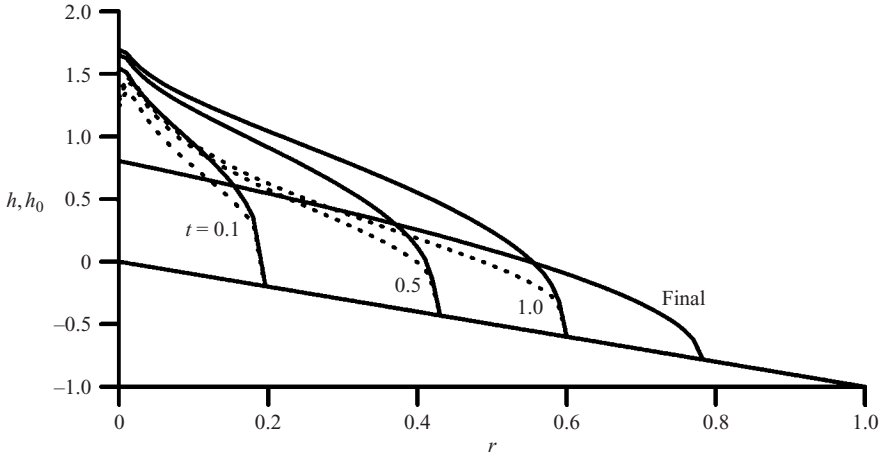


FIGURE 17. Time evolution of the free surface and the yield surface for $V_0 = 1$ and $Q_0 = 1$. The source is at $x_s = 0$, $y_s = 0$ (axisymmetric spreading). Solid line: free surface; dashed line: yield surface. The final free surface is at $t = 20$. The final yield surface coincides with the solid bottom.

https://doi.org/10.1017/S0022112004001478 Published online by Cambridge University Press

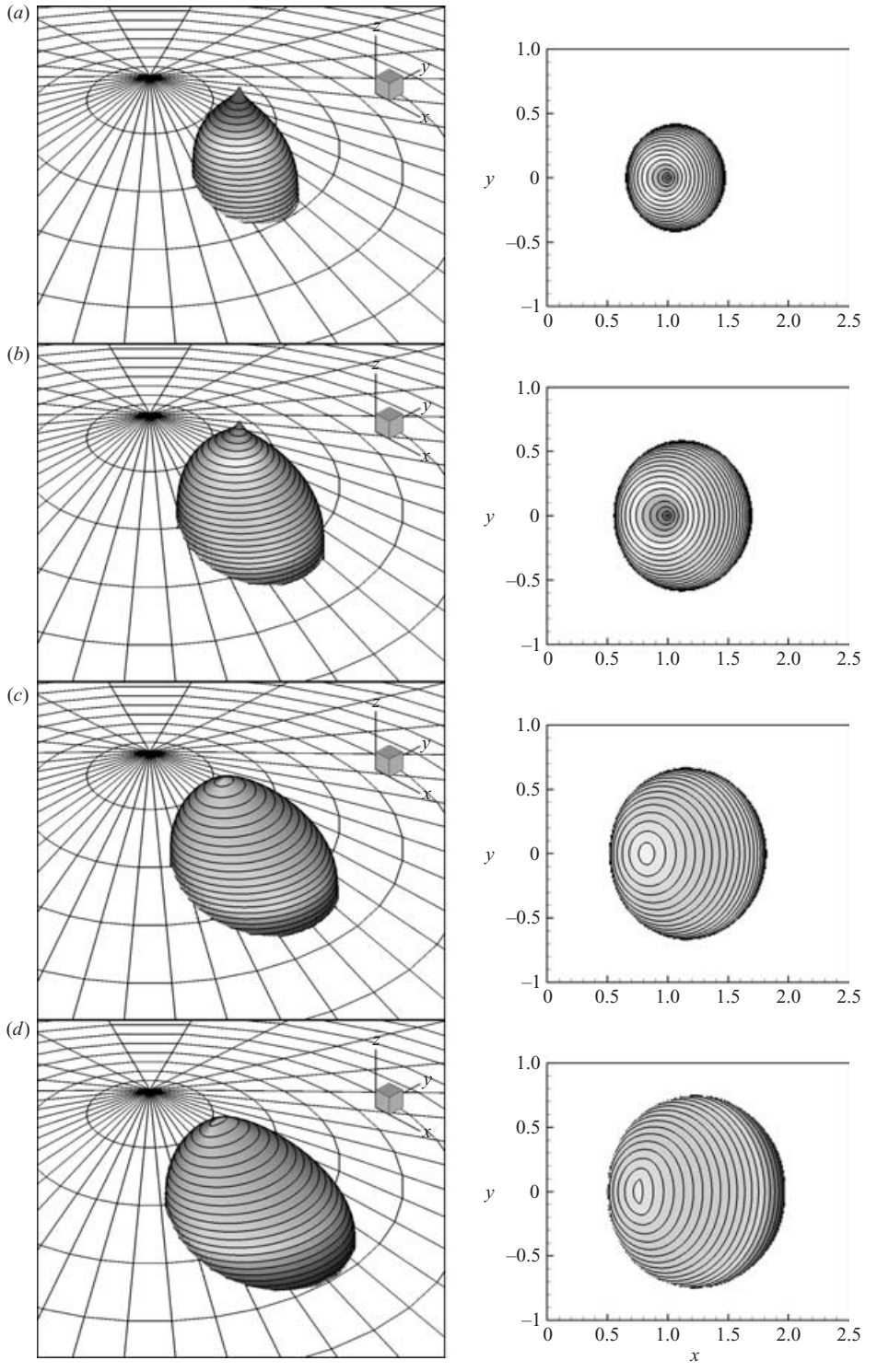


FIGURE 18. Mud spreading from a hillside for $V_0 = 1$ and $Q_0 = 1$. (*a*) $t = 0.5$, (*b*) 1, (*c*) 1.5, (*d*) 20. The source is at $x_s = 1$, $y_s = 0$. Mud is discharged until $t = 1$. In the right-hand column, the contour lines of the free-surface height are plotted with the interval $\Delta h = 0.1$. The highest contour is (*a*) $h = 0.7$, (*b*) $h = 0.8$, (*c*) $h = 0.2$, (*d*) $h = 0.1$, respectively.

https://doi.org/10.1017/S0022112004001478 Published online by Cambridge University Press

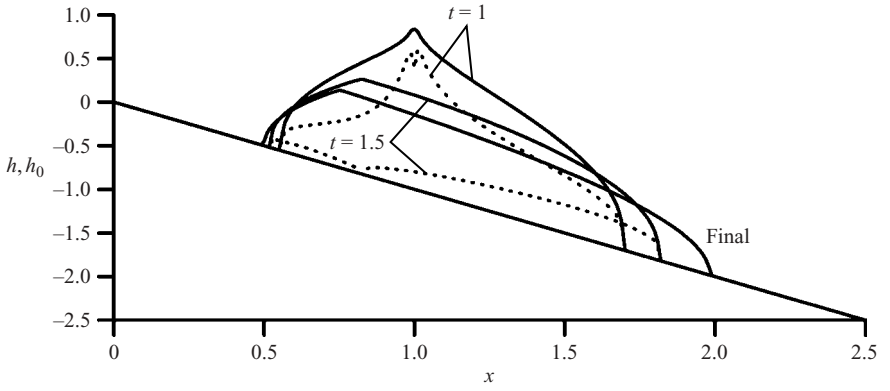


FIGURE 19. Time evolution of the free surface and the yield surface for $V_0 = 1$ and $Q_0 = 1$. The source is at $x_s = 1$, $y_s = 0$. Solid line: free surface; dashed line: yield surface. The final free surface is at $t = 20$. The final yield surface coincides with the solid bottom.

initial stage, the spreading is relatively uniform in all directions. Thus, it takes some time for the effect of the slope to influence the mud motion, as in the case of the basin. This was also noted in a high-speed gravity current (Ross, Linden & Dalziel 2002) and in a slow plastic flow down an inclined plane (Balmforth *et al.* 2002). After the initial stage, the down-slope advance of mud becomes more prominent. Unlike the flow into a basin, the front here is broad and the surface is everywhere convex; there is no shallow bowl on the free surface. The corresponding evolutions of the free surface and the yield surface along the centre plane are shown in figure 19. At the end of discharge, the pile has a single peak above the source. Since the free surface slope is small around the peak, there is a local depression of the yield surface. Then the fluid drains downhill rapidly, resulting in the upward shift of the peak after the discharge.

Similar computations have been carried out for various values of total volume, discharge rates, and discharge locations. The general trends are summarized here. For larger V_0 and fixed Q_0, or small Q_0 but fixed V_0, the pile is more elongated throughout the flow. If the volume is sufficiently large, the maximum width is attained near the front and the depth in the central region approaches the critical depth on an inclined plane (unity in dimensionless terms), as noted also in Coussot *et al.* (1996) and Balmforth *et al.* (2002). When the source is farther down from the hilltop, the results are, of course, closer to those for an inclined plan; the deposit is more elongated.

7. Summary remarks

In this paper, we have described the two- and three-dimensional slow spreading of a Bingham fluid over a gently sloped conical terrain. Under the lubrication approximation, a variety of axially symmetric profiles of threshold equilibrium have been derived analytically for both a conical basin and a conical hill. Simple formulae are derived for the mud profiles at the thresholds of equilibrium. Special features of Bingham plastics are pointed out, such as a surface depression over the peak of a submerged hill or a surface peak over the deepest point of a basin. Transient spreading of a finite fluid mass released from a point source has also been studied numerically. The effects of the total volume released and the discharge rate, etc., are investigated for both the final deposit and the transient evolution. In axisymmetric spreading, the final mud-front profile is shown to be independent of the total volume discharged and the

https://doi.org/10.1017/S0022112004001478 Published online by Cambridge University Press

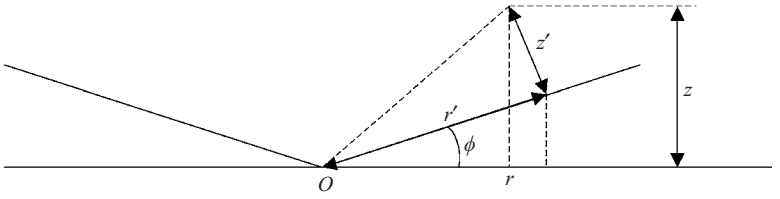


FIGURE 20. Relations between conical coordinates (r', θ', z') and cylindrical polar coordinates (r, θ, z). Only the vertical cross-section is shown. The azimuthal angle $\theta' = \theta$ is taken as in the ordinary polar coordinates.

discharge rate, despite the differences in the intermediate history. If mud is released on the hillside, however, the final profile of the asymmetric evolution depends on the flow history and on flow parameters such as the total volume released, discharge rate and the location of the source.

The results for the conical basin can be relevant for submarine mud slide. For a slow mud flow, water on top of the mud can be considered as inviscid and yields almost hydrostatically. The main effect of stratification is the change of gravity from g to $g' = (\rho' - \rho)/\rho$, as shown by Huppert (1982) in his Newtonian model of lava. For industrial purposes, it may be valuable to investigate the slow spreading of a shallow layer of mud over a steep conical surface. New analysis based on the equations in conical coordinates in the Appendix is desirable.

For predicting more catastrophic events associated with torrential rains or volcanic eruptions, it is important to study rapid flows on steep hillsides. Three-dimensional analysis of the inertial effects is challenging and awaits further investigation.

The present work is partially supported by a Grant-in-Aid for Scientific Research (no. 15560442) by the Japan Society for the Promotion of Science, for which M. Y. is grateful. M. Y. thanks Professor H. Ishida of Kanazawa University for his continued encouragement throughout this work. C. C. M. acknowledges the financial support of US National Science Foundation through Grant CTS-0075713 and US office of Naval Research Grant N00014-89-J-3128.

Appendix. Lubrication approximation on a conical surface with finite apex angle

In this Appendix, we first give the results of the lubrication approximation in conical coordinates for a shallow-layer flow over a cone of finite (arbitrary) apex angle. We then show that in the limit of small slope, the results are the same as obtained in § 2 by cylindrical coordinates.

Using the general theory of orthogonal curvilinear coordinates (see e.g. Hildebrand 1949), we first express the Navier–Stokes equations in the conical coordinates (r', θ', z') shown in figure 20, with r' being the radial distance along the bed from the origin (apex), z' the height normal to the conical bed, and θ' the polar angle. After the usual scalings for film flows under the assumptions

$$\frac{D'}{L'} \ll 1, \quad \tan\phi \leqslant O(1), \tag{A 1}$$

where D' and L' are the representative length scales in the z' and r' directions, respectively, the lubrication approximation is obtained. Finally, the continuity equation

https://doi.org/10.1017/S0022112004001478 Published online by Cambridge University Press

reads

$$\frac{1}{r'}\frac{\partial(r'u'_{r'})}{\partial r'}+\frac{1}{r'\cos\phi}\frac{\partial u'_{\theta'}}{\partial\theta'}+\frac{\partial u'_{z'}}{\partial z'}=0, \tag{A 2}$$

The momentum equations in the shear layer are reduced to

$$0=-\frac{1}{\rho}\frac{\partial p'}{\partial r'}-g\sin\phi+\nu\frac{\partial^2 u'_{r'}}{\partial z'^2}, \tag{A 3}$$

$$0=-\frac{1}{\rho r'\cos\phi}\frac{\partial p'}{\partial\theta'}+\nu\frac{\partial^2 u'_{\theta'}}{\partial z'^2}, \tag{A 4}$$

$$0=-\frac{1}{\rho}\frac{\partial p'}{\partial z'}-g\cos\phi. \tag{A 5}$$

It follows easily that the pressure is hydrostatic

$$p'=\rho g\cos\phi(h'-z'). \tag{A 6}$$

In the shear zone $0<z'<h_0$, the radial and azimuthal velocities are

$$u'_{r'}=-\frac{g}{2\nu}\left(\cos\phi\frac{\partial h'}{\partial r'}+\sin\phi\right)\left[h_0'^2-(h'_0-z')^2\right], \tag{A 7}$$

$$u'_{\theta'}=-\frac{g}{2r\nu}\frac{\partial h'}{\partial\theta'}\left[h_0'^2-(h'_0-z')^2\right]. \tag{A 8}$$

In the plug flow zone $h_0<z'<h$, the velocities are

$$u'_{r'p}=-\frac{g}{2\nu}\left(\cos\phi\frac{\partial h'}{\partial r'}+\sin\phi\right)h_0'^2, \tag{A 9}$$

$$u'_{\theta'p}=-\frac{g}{2r\nu}\frac{\partial h'}{\partial\theta'}h_0'^2. \tag{A 10}$$

Integrating the continuity equation with the help of boundary conditions and the velocity distribution, we obtain

$$\frac{\partial h'}{\partial t}+\frac{g}{\nu r'}\frac{\partial}{\partial r'}\left[\left(-\cos\phi\frac{\partial h'}{\partial r'}-\sin\phi\right)r'F'\right]+\frac{g}{\nu r'^2\cos^2\phi}\frac{\partial}{\partial\theta'}\left[\left(-\cos\phi\frac{\partial h'}{\partial\theta'}\right)F'\right]=0, \tag{A 11}$$

where

$$F'=\tfrac{1}{6}(3h'-h'_0)h_0'^2. \tag{A 12}$$

We now transform the preceding result to the upright cylindrical coordinates (r,θ,z), which are related to the conical coordinates by

$$r'=r\cos\phi+z\sin\phi,\quad \theta'=\theta,\quad z'=-r\sin\phi+z\cos\phi, \tag{A 13}$$

while the depth h' and h are related by

$$h'=-r\sin\phi+h\cos\phi. \tag{A 14}$$

In cylindrical coordinates, (A 11) becomes

$$\frac{\partial h}{\partial t}+\frac{g}{\nu r}\frac{\partial}{\partial r}\left[\left(-\frac{\partial h}{\partial r}-\tan^3\phi\right)rF\cos^6\phi\right]+\frac{g}{\nu r^2}\frac{\partial}{\partial\theta}\left[\left(-\frac{\partial h}{\partial\theta}\right)F\right]=0, \tag{A 15}$$

https://doi.org/10.1017/S0022112004001478 Published online by Cambridge University Press

where

$$F = \tfrac{1}{6}(3h - h_0 - 2H)(h_0 - H)^2. \tag{A 16}$$

These equations are valid for any finite inclination ϕ.

As a check for the approximation in § 2, we take the limit of (A 15) for small bottom slope ϕ, yielding

$$\frac{\partial h}{\partial t} + \frac{g}{\nu r}\frac{\partial}{\partial r}\left[\left(-\frac{\partial h}{\partial r}\right) rF\right] + \frac{g}{\nu r^2}\frac{\partial}{\partial \theta}\left[\left(-\frac{\partial h}{\partial \theta}\right) F\right] = 0, \tag{A 17}$$

which is equivalent to (2.4).

REFERENCES

Allersma, E. 1980 Mud in estuaries and along coasts. In *Proc. Intl Symp. River Sedimentation, Beijing, China*, pp. 663–685. Intl Research and Training Centre on Erosion and Sedimentation.

Balmforth, N. J., Burbidge, A. S., Craster, R. V., Salzig, J. & Shen, A. 2000 Visco-plastic models of isothermal lava domes. *J. Fluid Mech.* **403**, 37–65.

Balmforth, N. J., Burbidge, A. S. & Craster, R. V. 2001 Shallow lava theory. In *Geomorphological Fluid Mechanics* (ed. N. Balmforth & A. Provencale), pp. 164–187. Springer.

Balmforth, N. J. & Craster, R. V. 1999 A consistent thin-layer theory for Bingham plastics. *J. Non-Newtonian Fluid Mech.* **84**, 65–81.

Balmforth, N. J., Craster, R. V. & Sassi, R. 2002 Shallow viscoplastic flow on an inclined plane. *J. Fluid Mech.* **470**, 1–29.

Coussot, P. 1997 *Mudflow Rheology and Dynamics*. IAHR/AIRH Monograph.

Coussot, P. & Proust, S. 1996 Slow, unconfined spreading of a mudflow. *J. Geophys. Res.* **101**, 25 217–25 229.

Coussot, P., Proust, S. & Ancey, C. 1996 Rheological interpretation of deposits of yield stress fluids. *J. Non-Newtonian Fluid Mech.* **66**, 55–70.

Douglas, J. J. 1955 On the numerical integration of $\partial^2 u/\partial x^2 + \partial^2 u/\partial y^2 = \partial u/\partial t$ by implicit methods. *J. Soc. Ind. Appl. Maths* **3**, 42–65.

Griffiths, R. W. 2000 The dynamics of lava flows. *Annu. Rev. Fluid Mech.* **32**, 477–518.

Hildebrand, F. B. 1949 *Advanced Calculus for Engineers*. Prentice-Hall.

Huang, X. & Garcia, M. H. 1998 A Hersche–Bulkley model for mud flow down a slope. *J. Fluid Mech.* **374**, 305–333.

Hulme, G. 1974 The interpretation of lava flow morphology. *Geophys. J. R. Astrophys. Soc.* **39**, 361–383.

Huppert, H. 1982 The propagation of two-dimensional and axisymmetric viscous gravity currents over a rigid horizontal surface. *J. Fluid Mech.* **121**, 43–58.

Johnson, A. M. 1970 *Physical Processes in Geology*. Freeman Cooper.

Johnson, A. M. & Rodine, J. R. 1984 *Slope Instability* (ed. D. Brunsden & D. B. Prior), chap. 8. John Wiley.

Kang, C. C. 1996 *Debris Flow Hazards and their Control in China*. Science Press, Beijing, 118pp.

Krone, R. B. 1963 A study of rheological properties of estuarial sediments *Ser. Rep. 63-8*. Hydraulic Engineering Laboratory and Sanitary Research Laboratory, University of California, Berkeley.

Lipscomb, G. G. & Denn, M. M. 1984 Flow of Bingham fluids in complex geometries. *J. Non-Newtonian Fluid Mech.* **14**, 337–346.

Liu, K. F. & Mei, C. C. 1989 Slow spreading of a sheet of Bingham fluid on an inclined plane. *J. Fluid Mech.* **207**, 505–529.

Liu, K. F. & Mei, C. C. 1990 Approximate equations for the slow spreading of a thin sheet of Bingham plastic fluid *Phys. Fluids* A **2**, 30–36.

Liu, K. F. & Mei, C. C. 1994 Roll waves on a layer of a muddy fluid down a gentle slope – A Bingham model. *Phys. Fluids* **6**, 2577–2590.

McDowell, B. & Raymer, S. 1986 Eruption in Columbia. *Natl Geograph.* **169**, 640–653.

Mei, C. C., Liu, K. F. & Yuhi, M. 2001 Mud flows – slow and fast. In *Geomorphological Fluid Mechanics* (ed. N. Balmforth & A. Provencale), pp. 548–577. Springer.

https://doi.org/10.1017/S0022112004001478 Published online by Cambridge University Press

Mei, C. C. & Yuhi, M. 2001 Slow flow of a Bingham fluid in a shallow channel of finite width. *J. Fluid Mech.* **431**, 135–159.

Migniot, P. C. 1968 Étude de propriétés physiques de différents sediments tres fins et de leur comportment sous des action hydrodynamiques. *La Houille Blanche* **7**, 591–620.

Mileti, D. S., Bolton, P. A., Fernandez, G. & Updike, R. G. 1991 *The Eruption of Nevado Del Ruiz Volcano, Colombia, South America.* National Academy Press, Washington, DC.

Ng, C. & Mei, C. C. 1994 Roll waves on a shallow layer of mud modelled as a power-law fluid. *J. Fluid Mech.* **263**, 151–183.

Osmond, D. I. & Griffiths, R. W. 2001 The static shape of yield strength fluids slowly emplaced on slopes. *J. Geophys. Res.* **106(B8)**, 16 241–16 250.

Peaceman, D. W. & Rachford, H. H. 1955 The numerical solution of parabolic and elliptic differential equations. *J. Soc. Ind. Appl. Maths* **3**, 28–41.

Piau, J. M. 1996 Flow of a yield stress fluid in a long domain. Application to flow on an inclined plane. *J. Rheology* **40**, 711–723.

Pouliquen, O. & Forterre, Y. 2002 Friction law for dense granular flows: application to the motion of a mass down a rough inclined plane. *J. Fluid Mech.* **453**, 133–151.

Prager, W. 1961 *Introduction to Mechanics of Continua.* Ginn.

Qian, Y., Yang, W., Zhao, W., Cheng, X. & Zhang, L. 1985 Experimental study on homogeneous hyperconcentrated flow. In *Proc. Intl Workshop on Flow at Hyperconcentrations of Sediment, Beijing, China,* vol. 2.1, pp. 1–13.

Ross, A. N., Linden, P. F. & Dalziel, S. B. 2002 A study of three-dimensional gravity currents on a uniform slope. *J. Fluid Mech.* **453**, 239–261.

Takahashi, T. 1991 *Debris Flow.* IAHR/AIRH Monograph, Balkema, Rotterdam, 165pp.

Wang, Z. & Qian, Y. 1985 A preliminary investigation on the mechanism of hyperconcentrated flow. In *Proc. Intl Workshop on Flow at Hyperconcentrations of Sediment, Beijing, China,* vol. 2.4, pp. 1–13.

Wieland, M., Gray, J. M. N. T. & Hutter, K. 1999 Channelized free-surface flow of cohesionless granular avalanches in a chute with shallow lateral curvature. *J. Fluid Mech.* **392**, 73–100.

Wilson, S. D. R. & Burgess, S. L. 1998 The steady, spreading flow of a rivulet of mud. *J. Non-Newtonian Fluid Mech.* **79**, 77–85.

https://doi.org/10.1017/S0022112004001478 Published online by Cambridge University Press